Available online at www.sciencedirect.com
SCIENCE DIRECT®
Physics of the Earth and Planetary Interiors 155 (2006) 48–62
PHYSICS OF THE EARTH AND PLANETARY INTERIORS
www.elsevier.com/locate/pepi

Anisotropic structure of the African upper mantle from Rayleigh and Love wave tomography

Amal Sebai [a,b], Eléonore Stutzmann [a,*], Jean-Paul Montagner [a], Déborah Sicilia [a], Eric Beucler [c]

[a] *Département de Sismologie, Institut de physique du Globe de Paris, 4 place Jussieu, 75252 Paris Cedex 05, France*
[b] *CRAAG, BP 63, Bouzaréah, 16340 Alger, Algérie*
[c] *Laboratoire de Planétologie et Géodynamique, Université de Nantes, 2 rue de la Houssinière, BP 922O8, 44322 Nantes Cedex 3, France*

Received 2 May 2005; received in revised form 27 September 2005; accepted 27 September 2005

Abstract

The geodynamics of the mantle below Africa is not well understood and anisotropy tomography can provide new insight into the coupling between the African plate and the underlying mantle convection. In order to study the anisotropic structure of the upper mantle beneath Africa, we have measured phase velocities of 2900 Rayleigh and 1050 Love waves using the roller-coaster algorithm [Beucler, E., Stutzmann, E., Montagner, J.-P., 2003. Surface-wave higher mode phase velocity measurments, using a roller-coaster type algorithm. Geophys. J. Int. 155 (1), 289–307]. These phase velocities have been inverted to obtain a new tomographic model that gives access to isotropic S_V-wave velocity perturbations, azimuthal and radial anisotropies. Isotropic S_V-wave velocity maps have a lateral resolution of 500 km. Anisotropy parameters have a lateral resolution of 1000 km which is uniform over Africa for azimuthal anisotropy but decreases at the West and South of Africa for radial anisotropy. At shallow depth, azimuthal anisotropy varies over horizontal distances much smaller than the continent scale. At 280 km depth, azimuthal anisotropy is roughly N-S, except in the Afar area, which might indicate differential motion between the African plate and the underlying mantle.

The three cratons of West Africa, Congo and Kalahari are associated with fast velocities and transverse anisotropy that decrease very gradually down to 300 km depth. On the other hand, we observe a significant change in the direction and amplitude of azimuthal anisotropy at about 180 km depth, which could be the signature of the root of these cratons. The Tanzania craton is a shallower structure than the other African cratons and the slow velocities (−2%) observed on the maps at 180 and 280 km depth could be the signature of hot material such as a plume head below the craton. This slow velocity anomaly extends toward the Afar and azimuthal anisotropy fast directions are N-S at 180 km depth, indicating a possible interaction between the Tanzania small plume and the Afar. The Afar plume is associated with a very slow velocity anomaly (−6%) which extens below the Red sea, the Gulf of Aden and the Ethiopian rift at 80 km depth. The Afar plume can be observed down to our deepest depth (300 km) and is associated with radial anisotropy smaller than elsewhere in Africa, suggesting active upwelling. Azimuthal anisotropy directions change with increasing depth, being N-S below the Red sea and Gulf of Aden at 80 km depth and E–W to NE–SW at 180 km depth. The Afar plume is not connected with the smaller hotspots of Central Africa, which are associated either with shallow slow velocities for Mt Cameroon or with no particular velocity anomaly and N-S azimuthal anisotropy for the hotspots of Tibesti, Darfur and Hoggar. A shallow origin for these hotspots is in agreement with their normal 3He/4He ratio and with their location in a region that had been weakened by the rifting of West and Central Africa.
© 2005 Elsevier B.V. All rights reserved.

Keywords: Tomography; Anisotropy; Surface waves; Hotspot; Craton

* Corresponding author. Tel.: +33 1 4427 2413; fax: +33 1 4427 3894.
E-mail address: stutz@ipgp.jussieu.fr (E. Stutzmann).

0031-9201/$ – see front matter © 2005 Elsevier B.V. All rights reserved.
doi:10.1016/j.pepi.2005.09.009

1. Introduction

Africa is a large continent characterized by cratons, rift zones, volcanoes, swells, basins and broad plateaus. This variety of tectonic regions has evolved over the past 2 billion years, the oldest features being the cratons of West Africa, Congo, Tanzania and Kalahari (Fig. 1). During the Mesozoic, the Gondwana super continent broke up. About 200 My ago, the opening of the Central Atlantic Ocean separated West Africa and North America. Then, 183 My ago, South Africa was affected by the Karoo traps which initiated the separation of Madagascar, Antarctica and India from South East Africa (Storey, 1995). On the Atlantic side, the Mesozoic activity of St Helen hotspot (145 My) was probably linked to the development of several intra-continental rifts, the West African, Central African and Anza rift systems (Wilson and Guiraud, 1992). Further South, the Tristan da Cunha trap episode of Parana (South America) and Etendeka (Africa) occurred 133 My ago and was followed by the South Atlantic Ocean opening. The separation of South America and Africa was achieved 80 My ago. The shape of the African continent has not changed significantly since that time.

After a quiet period (80–30 My), volcanic activity started simultaneously in several regions of the African plate at hotspots characterized by a large variability in size and volcanic production (Burke, 1996). Small hotspots, such as Mount Cameroon, Hoggar, Tibesti and Darfur, were active during the Cenozoic and Quaternary with a modest volcanic production (Wilson and Guiraud, 1992). They appeared in regions that had been weakened by the rifting of West and Central Africa. On the other hand, Afar, Canary, Cape Verde hotspots had a much stronger activity and their volcanic eruptions are still observed today.

The Afar hotspot is located at a triple junction (Fig. 1). Two rifts have separated Arabia from Africa, with the opening of the Red Sea and the Gulf of Aden beginning, respectively, 30 and 20 My ago. The third rift system appeared within the African continent about 30 My ago and corresponds to the Ethiopia Rift which is connected to the East Africa Rift System (Burke, 1996). Courtillot et al. (1999) suggested that intra-continental rifting along the East African Rift has progressively stopped since 15 My ago while accretion was concentrated on the Gulf of Aden/Red Sea plate boundary. The Ethiopian and Yemen traps have long been associated with the Afar hotspot (Richards et al., 1989; White and McKenzie,

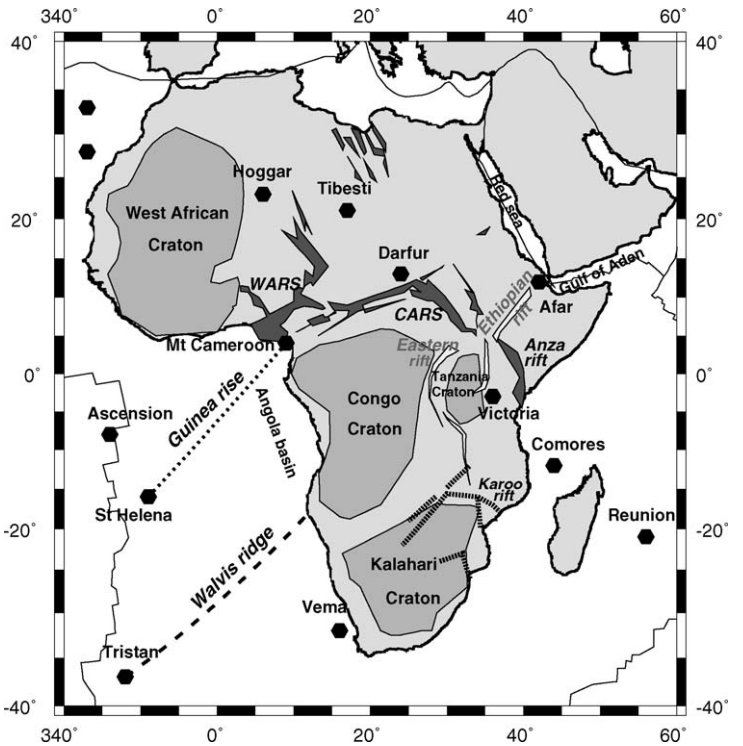

Fig. 1. Tectonic map of Africa. The West African (WARS), Central African (CARS) and Anza rift systems correspond to the Mesozoic rift basins. The Ethiopian and Eastern rifts are roughly 30 Ma old. Hotspots are plotted with black hexagons and cratons are in dark grey.

1989). The flood basalt eruption created a large elevated plateau 30 My ago, within 1 or 2 My (Hofmann et al., 1997). The continental area around the Afar region corresponds to a large region of low-density material associated with a negative Bouguer anomaly (Brown and Girdler, 1980; Hartley et al., 1996) and with slow seismic velocity anomalies in the upper mantle visible in all global tomographic models (e.g. Grand et al., 1997; Mégnin and Romanowicz, 2000; Ritsema and van Heijst, 2000a) and regional models (Hadiouche et al., 1989; Ritsema et al., 1998; Ritsema and Van Heijst, 2000b; Debayle et al., 2001). These observations suggest the existence of a hot and light plume rising in the mantle beneath the Afar. The relationship between Afar and the small hotspot of Darfur is debated. Hadiouche et al. (1989), who carried out the first surface wave tomography of the African plate with a lateral resolution of 2000 km, and later Ebinger and Sleep (1998), using geological and gravity data, suggested that Afar and Darfur might be connected to a single plume at depth. On the other hand, Burke (1996) and Wilson and Guiraud (1992) suggested that the Darfur, Tibesti and Hoggar, which correspond to Cenozoic alkali volcanism distributed over elliptical areas, are related to unconnected plumes.

Another striking feature of Africa is the existence of the large southern African plateaus that cover significant parts of the continent and are characterized by anomalous topography about 1000 m above the rest of the continent. Nyblade and Robinson (1994) linked these elevated regions to abnormally high bathymetry in the ocean in the south-eastern Atlantic Ocean. This broad elevated area has been named the African superswell (see Mc Nutt, 1998 for a review). Hager et al. (1985) and Lithgow-Bertelloni and Silver (1998) showed that the uplift may be supported by flow coming from the lower mantle. Indeed, the elevated area is located above a broad low velocity anomaly observed in the deepest part of the lower mantle on most global tomographic models, (e.g. Dziewonski, 1984; Ritsema et al., 1999; Romanowicz and Gung, 2002), and the upper mantle right below the superswell is characterized by high velocities. Ritsema et al. (1999) suggested that the low velocity anomaly originating in the deep mantle below South Africa, which they called a superplume, is deflected towards the northeast and reaches the surface in the Afar area. On the other hand, Davaille et al. (2005) argued, using fluid mechanics constraints, that the material erupting at Afar cannot come from the bottom of the mantle under South Africa. Instead, they propose that three instabilities occur along the same cross-section: a thermo-chemical banana shaped ridge under South Africa (Ni and Helmberger, 2003), a large hot upwelling to the northeast and a primary plume beneath the Afar whose connection to the bottom of the mantle might have already disappeared.

All current tomographic models of Africa are derived from Rayleigh surface waves (Hadiouche et al., 1989; Ritsema and Van Heijst, 2000a,b; Debayle et al., 2001) and display isotropic S_V-wave velocities which are interpreted in terms of fast/cold and slow/hot structures. In order to study the flow direction in the upper mantle, it is necessary to consider anisotropy parameters. If lattice preferred orientation (LPO) is the dominant cause of anisotropy in the upper mantle (e.g. Christensen and Lundquist, 1982; Nicolas and Christensen, 1987), the olivine fast axis is oriented along the maximum flow direction. In that case, radial anisotropy indicates whether the mantle flow is dominantly vertical or horizontal and azimuthal anisotropy can be related to the horizontal flow direction. Thus, both manifestations of anisotropy are necessary to constraint the mantle flow (Reagan and Anderson, 1984; Montagner, 2002). Accordingly, we present here the first regional tomographic model that includes both azimuthal and radial anisotropy. Azimuthal anisotropy is derived from Rayleigh wave phase velocity measurements and transverse anisotropy is obtained from the discrepancy between Rayleigh and Love wave propagation. This new model is used to study the connection between the upper mantle and the principal tectonic features of Africa. It also enables us to compare isotropic S-wave velocities with previous studies in order to quantify the effect of neglecting anisotropy in the tomographic procedure.

2. Data and method

2.1. Dataset

We considered earthquakes and broadband stations in and around the African plate (Fig. 2). The seismograms were recorded by 89 broadband stations from the GEOSCOPE, IRIS and MEDNET networks and temporary experiments including the French project “Horn of Africa”. We selected 1052 events with a magnitude *Ms* larger than 5.7 in the period 1982–2001. Due to the weak seismicity around the African plate, it was necessary to use earthquakes located further than the neighbouring plate boundaries, and therefore we also included events from the western and eastern Pacific coasts. The selection was performed manually to keep only data with a good signal to noise ratio. The final dataset consists of 2900 Rayleigh wave records and 1050 Love wave records selected from the vertical and transverse components of the long period channel (LH). The

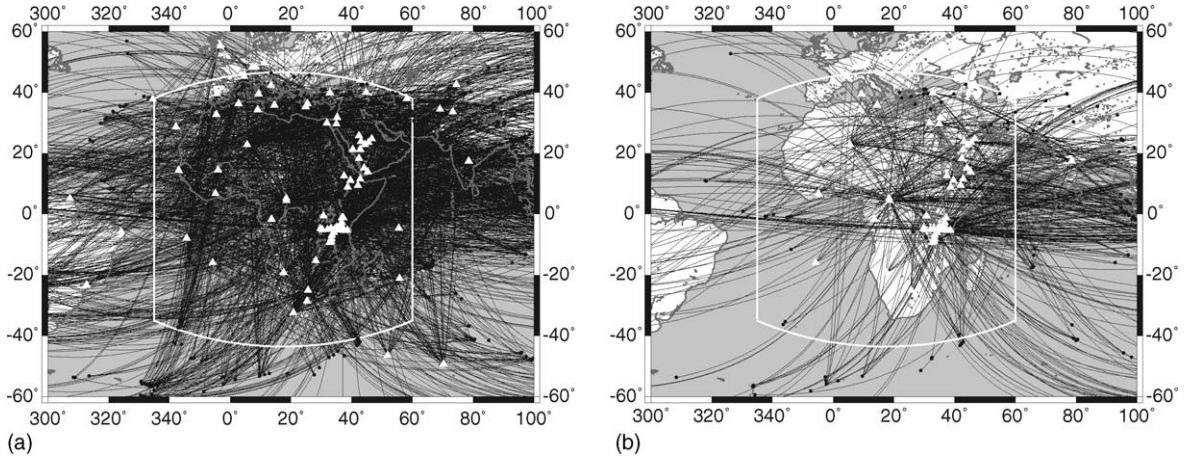

Fig. 2. Geographical distribution of the paths used in this study. (a) 2900 Rayleigh wave paths. (b) 1050 Love wave paths. Stations are plotted with triangles.

path distribution provides a good spatial and azimuthal coverage for Rayleigh waves beneath the entire African continent. For Love waves, the path coverage is good only beneath central and East Africa, as can be seen in Fig. 2.

2.2. Path by path phase velocity determination

Each waveform is compared with a synthetic seismogram computed by normal mode summation (Woodhouse and Girnius, 1982) using the Harvard centroid moment tensor solution. PREM is used as reference Earth model (Dziewonski and Anderson, 1981). The fundamental mode phase velocities of Rayleigh and Love surface waves are calculated for each path using the new roller-coaster technique developed by Beucler et al. (2003). This method is an improved version of the Fourier domain waveform inversion technique developed by Stutzmann and Montagner (1993). The forward problem can be written as follows for both Rayleigh and Love wave fundamental modes:

$$A_R(\Delta,\ \omega)\exp(i\,\Phi_R(\Delta,\ \omega)) = A_s(\omega)\exp\left[i\left(\Phi_S(\omega) - \omega\Delta\, n_s\left(1+\frac{\delta n}{n_s}\right)\right)\right] \quad (1)$$

where A_R and Φ_R are the amplitude and phase of the real data spectrum, Δ is the epicentral distance in km, and ns is the fundamental mode phase slowness at frequency ω computed in the reference model and $\delta n/n_s$ the relative slowness perturbation that we want to retrieve. A_s and Φ_S are amplitude and phase terms that include the source term, the geometrical spreading and the receiver response.

The phase velocity determination is non unique, in most cases due to a 2π ambiguity as can be seen from Eq. (1). To deal with this problem, the roller-coaster method determines the dimensionless slowness perturbation $\delta n/n_s$ in two steps. Considering simultaneously the entire frequency range, we first determine all possible slowness perturbation that are solutions of Eq. (1) with smooth variations as a function of frequency around the reference model. Each of these smooth slowness perturbation curves is then used as starting parameter in a least square inversion (Tarantola and Valette, 1982). Among the least square solutions, we keep the slowness perturbation curve that corresponds to the minimum misfit. The computation of the a posteriori covariance matrix (Tarantola and Nercessian, 1984) makes it possible to take into account the reliability of the measurement which varies as a function of the data amplitude at a given frequency. Thus, we estimate the phase velocity measurement error, σ_d.

Rayleigh and Love wave phase velocities are calculated in the entire period range 45–250 s. This period range does not allow resolution of crustal structure, though the latter has a significant influence on phase velocities even at long period (Montagner and Jobert, 1988; Stutzmann and Montagner, 1994). Therefore, shallow layer phase velocity corrections are computed by using the CRUST2 model (upgrade of CRUST5.1 model, Mooney et al., 1998) and they are subtracted from the measurements path by path. The shallow layer model includes crust and sediment velocity and thickness, and topography. We have tested the influence of the crust model on our tomographic model by considering the two $2^\circ \times 2^\circ$ shallow layer models 3SMAC (Nataf and Ricard, 1996) and CRUST2. For both models, we have computed

phase velocity maps after crust correction along each path. We concluded that for Africa, there is no significant change in the phase velocity corrections between these two models because both models have similar shallow structure, primarily because the thickness of the crust is not well constrained below Africa. Shallow layer corrections increase the velocity contrast between ocean and continent. They increase phase velocities beneath continents (+2% to +0.5% for Rayleigh waves at periods between 45 and 250 s) and decrease them beneath oceans (−2% and −0.5% for Rayleigh waves at periods of 45 and 250 s, respectively). Their effect is even larger for Love waves, with an average velocity increase of +4% to +1% beneath Africa for periods between 45 and 250 s and an average velocity decrease of −3% to −1% beneath oceans.

2.3. Regionalization

Lateral phase velocity variations are computed by using the regionalization method developed by Montagner (1986). One advantage of this technique is that it allows zooming on a specific area where the path coverage is very dense. Following the approach of Smith and Dahlen (1973), the local azimuthally varying phase velocity $C(\omega, M, \Psi)$ is expressed, at location M, for each angular frequency ω and azimuth Ψ, as follows:

$$C(\omega, M, \psi) = C_{\mathrm{REF}}(\omega)[1 + a_0(\omega, M) + a_1(\omega, M)\cos 2\psi + a_2(\omega, M)\sin 2\psi + a_3(\omega, M)\cos 4\psi + a_4(\omega, M)\sin 4\psi] \quad (2)$$

Here C_{REF} is the reference model phase velocity, and the parameters a_0 and a_i (with $i = 1$–4) are, respectively, the isotropic phase velocity perturbation and the azimuthal anisotropy coefficients. Using the least square inversion algorithm of Tarantola and Valette (1982), the inversion for retrieving ai ($i = 0$–4) is controlled by three parameters: the phase velocity measurement error σ_{d}, (see Section 2.2), the a priori parameter errors, σ_{p}, and the correlation length, L. σ_{p} gives a constraint on the anomaly amplitude and L acts as a smoothing criterion. They are used to define the a priori covariance matrix for the parameters, C_{p}:

$$C_{\mathrm{P}}(M_1, M_2) = \sigma_{\mathrm{P}}(M_1)\sigma_{\mathrm{P}}(M_2)\exp\left[\frac{\cos\Delta - 1}{L^2}\right] \quad (3)$$

where Δ is the distance between two points M_1 and M_2 on the Earth.

Optimal values for σ_{p} and L are determined by a series of tests with synthetic data in which the model misfit is compared with the input errors. The spatial resolution is related to the number of paths covering the area of interest and to the frequency. To invert Rayleigh and Love wave phase velocities, we have selected a correlation length of 400 km and a priori errors on the parameters of 5% for the isotropic term and 2% for the anisotropy. Our measurements correspond to phase velocities in the period band 45–250 s. For ideal path coverage, phase velocities measured at a period of 45 s allow recovery of shallow structures of about 200 km wide whereas 250 s period phase velocities are sensitive to deeper structure with lateral resolution of about 1000 km. Our path coverage enables recovery of lateral structure 500 km wide, but we have to keep in mind that the sensitivity of surface waves causes the resolution to decrease with depth. Synthetic tests (Appendix A) show that, for Rayleigh wave path coverage, lateral variations of 500 km × 500 km and 1000 km × 1000 km are correctly recovered for isotropic-velocity and azimuthal anisotropy, respectively, with almost no trade-off between isotropic-velocity and anisotropy recovery. For Love waves, because the path coverage is good only in central and east Africa, anomalies of 1000 km × 1000 km can only be recovered in that area and radial anisotropy will not be considered elsewhere in Africa.

2.4. Phase velocity maps

Montagner and Nataf (1986) have shown that Rayleigh wave phase velocities are mainly sensitive to azimuthal anisotropy through the 2Ψ terms (coefficients a_1 and a_2 of Eq. (2)) whereas Love wave phase velocities are mainly sensitive to the 4Ψ terms (coefficients a_3 and a_4 of Eq. (2)). Due their rapid azimuthal variation, the 4Ψ coefficients are not well resolved. We invert for them so as not to bias the other terms of the expansion, but we present only anisotropy perturbations derived from the 0–2Ψ terms for Rayleigh wave and the a_0 coefficient for Love waves.

The Rayleigh wave phase velocity maps are presented in Fig. 3 for periods of 70 and 150 s, together with their error maps. The errors are around 1% and never exceed 2% below the Africa. At 70 s, maximum positive velocity perturbations of 6–7% are associated with the cratons of West Africa, Congo, Kalahari, Tanzania and Arabia. These anomalies are still visible at 150 s but with smaller amplitude (3–4%). The strongest negative anomaly (−6.5%) is located in the Afar region. This slow velocity anomaly extends toward the North

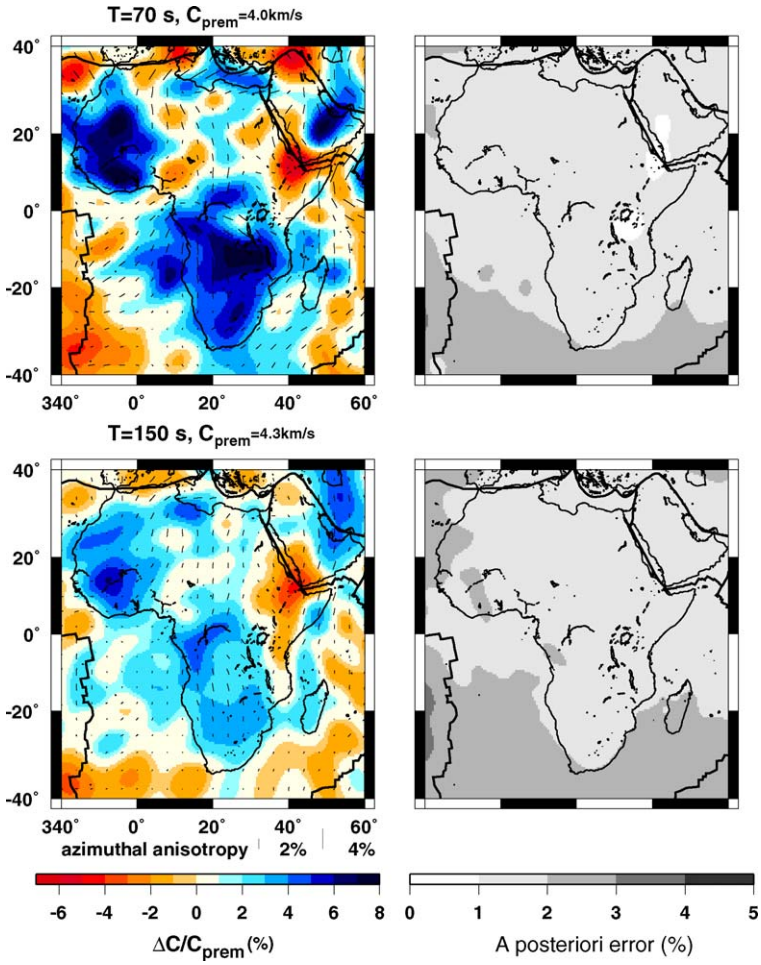

Fig. 3. Left: Rayleigh phase velocity perturbation maps with respect to the PREM model obtained after correction for the shallow layers. Bars correspond to fast anisotropy directions. Hotspots are plotted with black hexagons. Right: a posteriori errors on velocities.

beneath the Red Sea, toward the East beneath the Gulf of Aden and toward the South beneath the Anza rift system. At 150 s period, the Afar slow velocity anomaly amplitude decreases to −4%, and it can be followed further South than at shorter period. The West African Rift (WARS) area is also slow at 70 s (−3%) and the slow velocity anomaly vanishes close to 150 s period. Finally, slow velocities are also observed underneath the Atlantic Ocean ridge at 70 s period.

Azimuthal anisotropy of Rayleigh wave phase velocity is plotted on Fig. 3 where the bar direction indicates the fast direction and the bar length is proportional to the anisotropy amplitude. The anisotropy amplitude decreases with increasing period. We observe significant change in anisotropy direction between 70 and 150 s period, in East Africa and beneath the cratons.

Love wave phase velocity maps are presented on Fig. 4 for periods of 80 and 150 s. Since the number of paths is smaller for Love waves than for Rayleigh waves, the lateral resolution is poorer in the former case and the associated errors are larger, particularly in the southern part of the map (Fig. 4), where the Kalahari craton is not visible at 80 s period due to the lack of azimuthal coverage. Therefore, Love wave phase velocities are only interpreted beneath central and east Africa. In that well resolved area, the principal features are similar for both Love and Rayleigh wave maps. The Congo and Arabia cratons are associated with positive anomalies in the whole period range. A strong negative anomaly is located in the Afar region and extends beneath the Red Sea and the Gulf of Aden at every period.

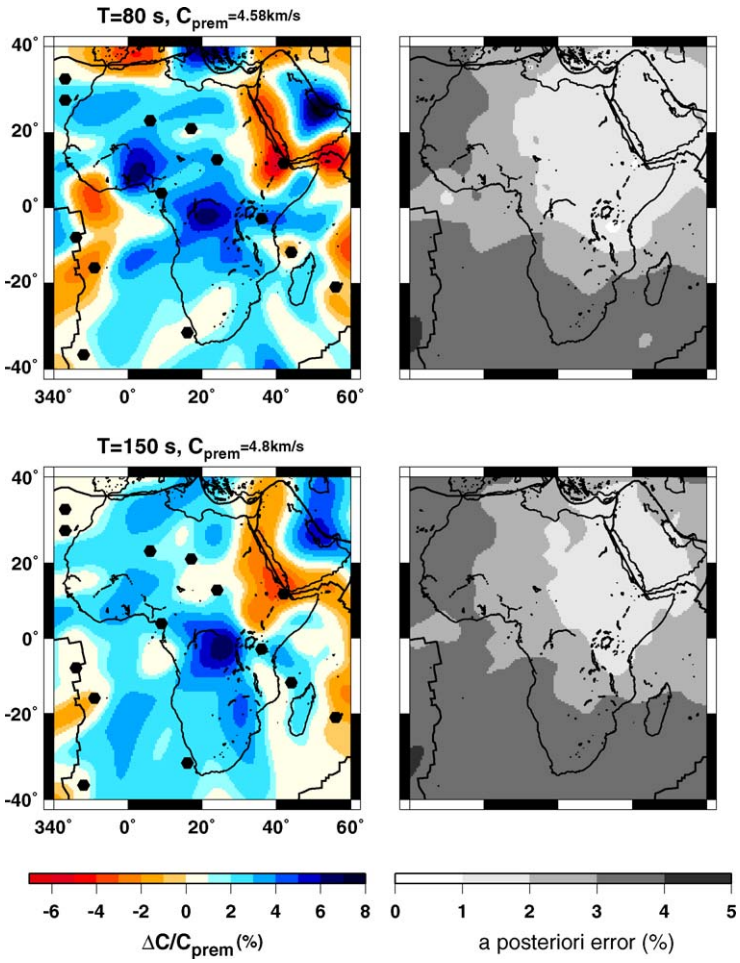

Fig. 4. Left: Love phase velocity perturbation maps with respect to the PREM model obtained after correction for shallow layers. Right: a posteriori errors on phase velocities.

2.5. S-wave velocity inversion

Following Montagner and Nataf (1986), a general anisotropy can be described by 13 parameters. The five parameters (A, C, F, L, N) describe the equivalent transverse isotropic medium with a vertical symmetry axis and correspond to the average over all azimuths. The other six parameters $B_{s,c}$, $G_{s,c}$, $H_{s,c}$ describe the 2Ψ azimuthal variations of A, L and F whereas the two parameters $E_{s,c}$ define the 4Ψ variations of A or N.

The Rayleigh wave phase velocity perturbation, δCR (M, T, Ψ) is expressed at location M for each period T and azimuth Ψ as follows:

$$\delta C_R(M, T, \psi) = \int_0^A \left[\frac{\partial C_R}{\partial A}(\delta A + B_c \cos 2\psi + B_s \sin 2\psi + E_c \cos 4\psi + E_s \sin 4\psi) + \frac{\partial C_R}{\partial C}\delta C + \frac{\partial C_R}{\partial F}(\delta F + H_c \cos 2\psi + H_s \sin 2\psi) + \frac{\partial C_R}{\partial L}(\delta L + G_c \cos 2\psi + G_s \sin 2\psi) \right] \frac{dz}{\Delta h} \quad (4)$$

Similarly for Love wave phase velocity perturbations, δC_L (M, T, Ψ), we have:

$$\delta C_L(M, T, \psi) = \int_0^a \left[\frac{\partial C_L}{\partial L}(\delta L - G_c \cos 2\psi - G_s \sin 2\psi) + \frac{\partial C_L}{\partial N}(\delta N - E_c \cos 4\psi - E_s \sin 4\psi) \right] \frac{dz}{\Delta h} \quad (5)$$

The kernels $\partial C_L/\partial p_i$ are calculated in the spherically symmetric reference model PREM. The inverse problem is resolved by using a least square inversion algorithm (Tarantola and Valette, 1982). The errors on phase velocities obtained from the regionalisation procedure are taken into account and the final error on the parameters is estimated by computing the "a posteriori" covariance matrix. The model is described by 20 km thick layers and a Gaussian correlation between adjacent layers is introduced. The inversion is performed using the 13 parameters per layer but only four parameters are well resolved: L, N, G_c and G_s. Therefore, only the following parameters of the 3D model are presented as a function of depth:

$$V_{sv} \approx \sqrt{\frac{L + G_c \cos 2\psi + G_s \sin 2\psi}{\rho}} \quad (6)$$

$$\xi \approx \left(\frac{V_{SH}}{V_{SV}}\right)^2 \approx \frac{N}{L} \quad (7)$$

where V_{SV} is the S_V-wave velocity and V_{SH} is the S_H-wave velocity.

3. Anisotropic 3D tomographic model

The anisotropic S_V-wave velocity model is shown on Fig. 5a, at 80, 180 and 280 km depths. The corresponding errors are between 1.3 and 2% at every depth (Fig. 5b). A good correlation is observed between velocity anomalies and tectonic features. The strongest positive velocity anomalies correspond to cratons, whereas the strongest negative anomaly is located beneath the Afar triple junction area. Azimuthal anisotropy fast directions of S_V-waves are plotted with bars on Fig. 5a. North of the equator in central Africa, anisotropy directions are to first order North-South at every depth, whereas elsewhere we observe variations of the fast direction laterally and with increasing depth. Azimuthal anisotropy varies over horizontal distances much smaller than the continent scale and therefore we do not observe a clear correlation with the present day absolute plate motion (APM). This is in agreement with the global study of Debayle et al. (2005) which showed that among all continents, only the Australia displays a strong correlation between azimuthal anisotropy and APM. The African plate motion is very slow and so the lack of correlation between azimuthal anisotropy and APM is not surprising. Nevertheless, the mapping of azimuthal anisotropy shows a large scale North-South direction below the continent at 280 km depth, except in the Afar area, which might indicate differential motion between the African plate and the mantle underlying convection. Radial anisotropy is plotted along two cross-sections on Fig. 6. We observe that radial anisotropy is weaker beneath the Afar than elsewhere in Africa.

4. Discussion

In this section, we discuss the relationship between the principal tectonic features of Africa and the upper mantle anisotropic structure.

4.1. Cratons

The strongest positive velocity anomalies with respect to the PREM model correspond to the four cratons of West Africa, Congo, Tanzania and Kalahari (Figs. 5 and 6). For all the African cratons except that of Tanzania, the maximum velocity perturbation is 5% at 80 km depth and decreases gradually to 3.5% at 180 km depth and around 1% at 280 km depth. Radial anisotropy within the cratons is larger than 1.1 and also decreases gradually with increasing depth (Fig. 6).

In the West African craton, the anisotropy fast direction at 80 km depth is North-South in its northern part and rotates further south to become parallel to the Guinea rise and the WARS. At 180 km depth, the azimuthal anisotropy amplitude is small and increases with depth to around 3% at 280 km depth along a North-South direction. In the Congo craton, the anisotropy fast direction is NW-SE at 80 km and it becomes gradually North-South at 280 km depth. Similarly to the West African craton, anisotropy amplitude is small around 180 km and increases again at 280 km. In the Kalahari craton, anisotropy is along a North-South direction at 80 km depth and the anisotropy amplitude is weak below 180 km depth. For the three cratons, we observe a gradual decrease of the velocity amplitude and of radial anisotropy with depth down to 300 km (Fig. 6) and a significant change of the anisotropy amplitude and direction around 180 km depth. The azimuthal anisotropy change around 180 km depth may be the signature of the craton root.

The Tanzania craton is surrounded by the eastern and western branches of the East African Rift. Synthetic tests (Appendix A) show that an isotropic structure 500 km wide (about the size of the Tanzania craton) can be resolved in our model, but not anisotropy variations. At 80 km depth, the Tanzania craton is associated with fast velocities but at 180 km depth, fast velocities are only observed at its western edge which suggests that it is shallower than the

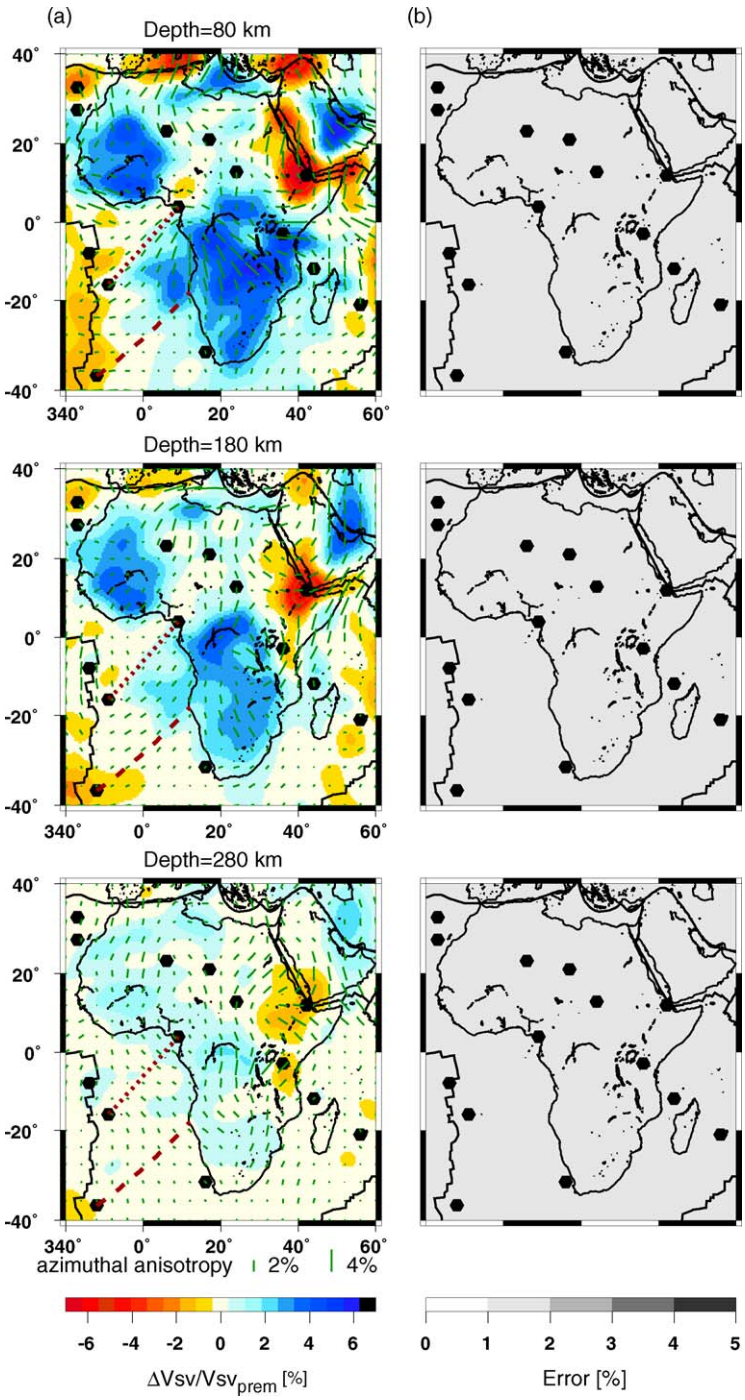

Fig. 5. (a) Lateral variations of S_V-wave velocity with respect to PREM at depth 80 km (top), 180 km (middle) and 280 km (bottom). The bars correspond to the directions of fast velocity. (b) A posteriori error.

other three African cratons. Its shallower root can be explained by the tectonic activity that affected the Tanzania craton while the other three cratons were in stable areas. That depth is consistent with the results of Zhao et al. (1999) who measured body wave travel times from a temporary regional array and found fast S-wave velocities only down to about 180 km depth. Weeraratne et al. (2003) also obtained fast velocities down to 150–180 km depth from high-resolution Rayleigh wave tomography using a regional array of

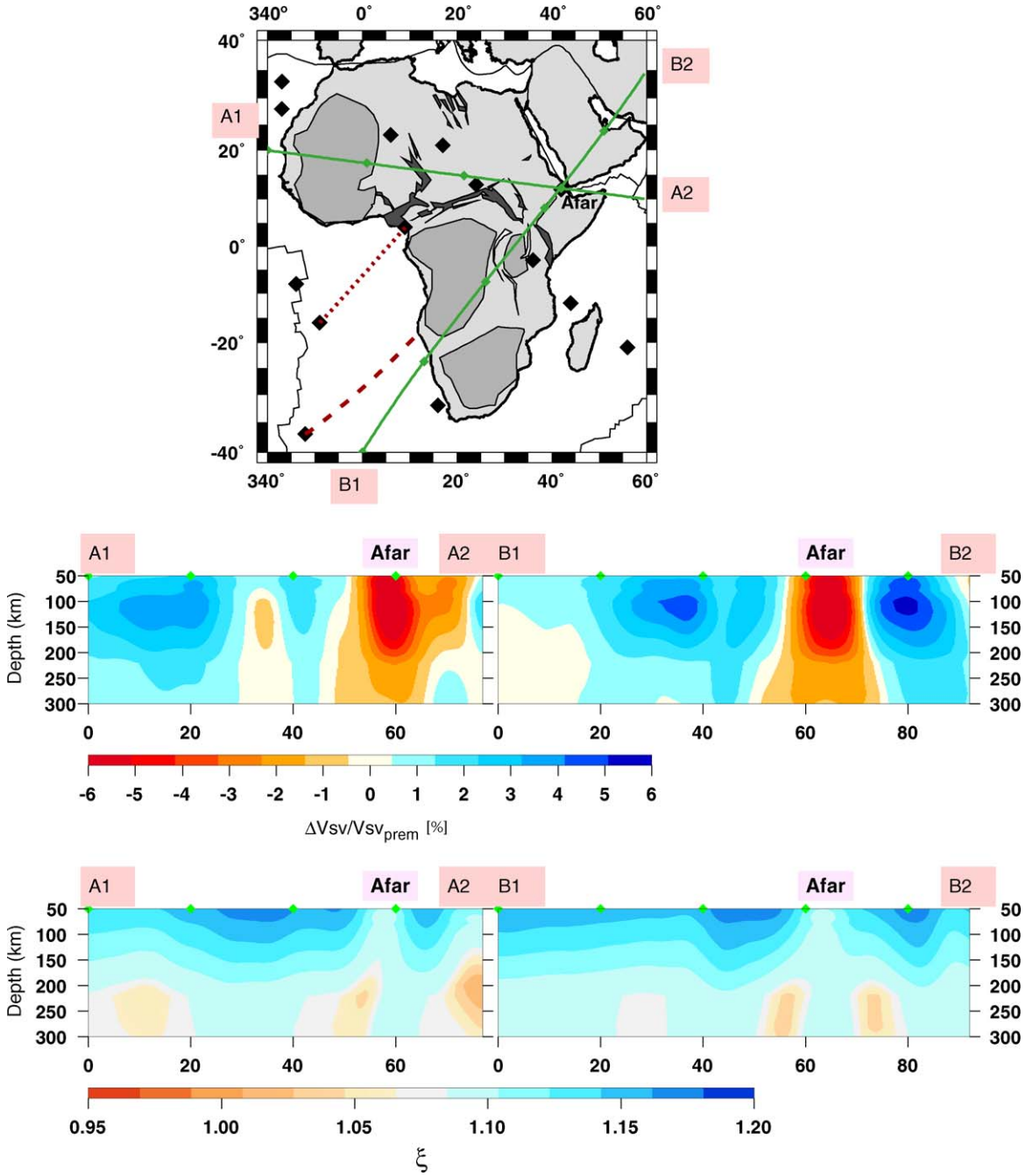

Fig. 6. Tectonic map of Africa showing the cross-section paths A1–A2 (left) and B1–B2 (right). Distances (°) along cross-sections are plotted on the horizontal axis. (a) Cross-section of isotropic S_V-velocity anomalies. (b) Cross-section of radial anisotropy.

stations in Tanzania. They also present evidence for anomalously low velocities beneath the cratonic lithosphere which they interpret as the signature of a plume rising beneath the craton. Though our model has less resolution than their local tomographic model, we also observe slow velocities under and east of the Tanzania craton. In our model, the slow velocity anomaly is larger than the Tanzania craton and it extents towards the North at 180 km depth. It is discussed in Section 4.3.

4.2. Beneath the superswell

South of the Equator, the broad area of positive velocity anomaly visible at 80 km depth includes the South African cratons and extends into the Atlantic Ocean between the Guinea rise and the Walvis ridge beneath the Angola basin. The fast anomaly is shallower beneath the ocean than beneath Africa and disappears below 200 km depth. This fast anomaly seems to be limited by the two hotspot tracks of St Helen at the North and Tristan at the South.

This wide fast anomaly south of the equator (Fig. 5) is located below the broad area of high topography in Africa that is prolonged into the ocean by a zone of elevated bathymetry called the African superswell (see Mc Nutt, 1998 for a review). Nyblade and Robinson (1994) used the residual topography to locate the zone of elevated bathymetry in a narrow zone at the South of Walvis rise. In our tomographic model (Fig. 5), that area is associated with fast velocities at 80 km depth of smaller amplitude than further North in the eastern South Atlantic Ocean. Below the continent, our model shows fast velocities below the entire superswell down to about 280 km depth, except in South East Africa where we observe fast velocities only down to 180 km depth and slow velocities deeper. Hager et al. (1985), Lithgow-Bertelloni and Silver (1998) and Gurnis et al. (2000) estimated density variations by scaling a global shear velocity model and computed the mantle flow beneath South Africa. They showed that southern Africa is actively being uplifted by a positively buoyant structure within the lower mantle and that there is no need for a shallow slow velocity anomaly to explain the excess elevation of the superswell. This is compatible with the fast velocities that we observe in the lithosphere beneath the superswell (Fig. 5) and with a radial anisotropy cross-section (Fig. 6, cross-section B1–B2) where V_{SH} is larger than V_{SV}, similarly to elsewhere in Africa except in the Afar area.

4.3. East Africa and the Afar plume

The Afar area corresponds to the strongest negative S-wave velocity anomaly (Figs. 5 and 6). At 80 km depth, the maximum negative anomaly (−6%) is observed beneath the Afar triple junction. The area of slow velocity follows the shape of the Red sea and the Aden Gulf and also extends below the Ethiopian rift. With increasing depth, the maximum amplitude decreases from −6% at 80 km depth to −4.5% at 180 km. At that depth, the slowest velocity anomaly in still centred below the Afar triple junction. Slow velocities (−2%) are also observed further South than at shallower depth whereas the anomaly size along the Red Sea and the Gulf of Aden is decreasing. At 280 km depth, the slow velocity anomaly (−1.5%) is still visible. It is slightly shifted toward the West with respect to the Afar triple junction and we observe also slow velocities below Tanzania, as already mentioned.

At 80 km depth, the azimuthal anisotropy fast direction is North-South below the Red sea and the Gulf of Aden and E-W below the Ethiopian rift and Tanzania. At 180 km depth, these directions change and become North-South south of Afar. Cross-sections show that radial anisotropy is smaller beneath Afar than elsewhere in Africa. The low radial anisotropy area is narrower than the slow velocity region (Fig. 6).

The Afar area is currently the most active volcanic area of Africa. The triple junction connects the two rifts responsible for the opening of the Red Sea and Aden Gulf and the East African Rift (Burke, 1996; Fig. 1). The strong negative anomaly and the weak radial anisotropy that we observe in this area are consistent with active mantle upwelling, as suggested by Camp and Roobol (1992). The depth extent of the slow velocity suggests that a plume is rising from below 300 km depth, which is consistent with the results of Debayle et al. (2001). We cannot resolve deeper structure, but Marty et al. (1993, 1996) showed that Afar lavas have 3He/4He ratio higher than those sampled along mid-ocean ridge. They interpret this high ratio as the signature of a lower mantle component. Moreover, Davaille et al. (2005) argued, using global tomography and fluid mechanics constraints, that the Afar is a primary plume (Courtillot et al., 2003) whose connection to the bottom of the mantle would have already disappeared.

Weeraratne et al. (2003) suggested the existence of another plume beneath the Tanzania craton. Rogers et al. (2000) showed that basalts erupted in Kenya have distinct Nd and Sr isotopic compositions distinct from basalts associated with the Afar plume suggesting a different plume. In that same region, Marty et al. (1996) showed that lavas have a 3He/4He ratio between 6 and 9 Ra, consistent with a shallower origin than the Afar plume (Montagner et al., submitted for publication). In our model, we observe fast velocity anomalies below Tanzania at 80 km depth, an elongated slow velocity anomaly at 180 km, which becomes more circular at 280 km depth. Its amplitude is small, around −1%, the azimuthal anisotropy is along a North-South direction at 180 km depth and radial anisotropy is larger than close to the Afar area. Both the velocity anomaly and azimuthal anisotropy suggest that this plume might interact with the Afar plume at 180 km depth, but that it is clearly

associated with a much weaker mantle upwelling than the Afar plume.

4.4. Rifting zone and hotspots in Central Africa

In Central Africa, velocity anomalies are weak compared to the cratons and the Afar area. We observe slow velocities (−1.5%) close to the Mt Cameroon hotspot at 80 km depth, and this anomaly disappears around 180 km depth. Anisotropy fast direction seems to follow the West African Rift system. Further east, we also observe a North-South band of 1% fast velocity between the Tibesti and Darfur hotspots, and the anisotropy direction is roughly North-South. Central Africa was affected by tectonic activity until the Quaternary. The Central African rift was active between 130 and 80 My. After a quiet period, volcanoes erupted in this area already weakened by the rifting and the hotspots of Mount Cameroon, Hoggar, Tibesti and Darfur have been active from 30 to 1 My (Wilson and Guiraud, 1992). Tomographic maps show that only Mt Cameroon is associated with a shallow negative anomaly and that Hoggar, Tibesti and Darfur have no particular seismic signature in the upper mantle, suggesting that there is no deep mantle upwelling in the area and no connection with the Afar plume. A similar conclusion was obtained by Ayadi et al. (2000) who used a linear array of short period stations and obtained slow velocities down to 200 km in a 100–200 km wide area below the Hoggar swell. Such a narrow anomaly cannot be seen by our surface wave tomography. Plumes being transient phenomena, the lack of a deep slow velocity anomaly may indicate an asthenospheric origin of these hotspots or the gradual cooling of a deeper plume (Silveira et al., in press). In the case of these Central Africa hotspots, a shallow origin is consistent with the 3He/4He ratio between 6 and 9 Ra measured close to Cameroon, Hoggar and Darfur (Montagner et al., submitted for publication).

5. Conclusion

In order to study the flow directions in the upper mantle, we present the first regional tomographic model that includes both azimuthal and radial anisotropy. Azimuthal anisotropy is derived from Rayleigh wave phase velocity measurements and radial anisotropy is obtained from the discrepancy between Rayleigh and Love wave propagation. Isotropic S_V-wave velocity maps have a lateral resolution of 500 km. Anisotropy parameters have a lateral resolution of 1000 km that is uniform over Africa for azimuthal anisotropy but decreases at the West and South of Africa for radial anisotropy. At shallow depth, azimuthal anisotropy varies over horizontal distances much smaller than the continent scale but on the map at 280 km depth, azimuthal anisotropy is roughly North-South, except in the Afar area, which might indicate differential motion between the African plate and the underlying mantle.

The strongest positive velocities correspond to the West Africa, Congo and Kalahari cratons and are visible down to 300 km depth. Whereas velocities and radial anisotropy gradually decrease with increasing depth, there is a significant change of azimuthal anisotropy amplitude and direction around 180 km depth which might indicate the base of the cratons. The Tanzania craton is shallower and fast velocity anomalies are observed only down to 180 km depth. Below, we observe slow velocities which could be the signature of a plume as suggested by Weeraratne et al. (2003).

The slowest velocities correspond to the Afar plume, the currently the most active area of Africa. The Afar plume conduit is visible down to the deepest depth inverted (300 km) and is associated with weak radial anisotropy, suggesting active upwelling whose origin is too deep to be resolved by our model. Both the velocity anomaly maps and the North-South azimuthal anisotropy at 180 km depth suggest that it might interact with the smaller Tanzania plume.

In central Africa, tomographic maps show that only Mt Cameroon is associated with a shallow negative anomaly and that Hoggar, Tibesti and Darfur have no seismic signature in the upper mantle, suggesting an asthenospheric origin for these hotspots. Radial anisotropy is larger than beneath Afar and azimuthal anisotropy is North-South in central Africa, confirming that these hotspots have no connection with the Afar plume.

Acknowledgments

This is IPGP contribution number 2097. The authors would like to thank A. Davaille for fruitful discussions and the two anonymous reviewers for their detailed comments.

Appendix A. Resolution tests

In order to estimate the lateral resolution of our model, we used checkerboard tests. We constructed synthetic phase velocities for the real path coverage. The inversion was performed with the same correlation length (400 km) and a priori errors as in the real case. The resolution is considered good when the checkerboard image is reconstructed. Fig. 7 illustrates

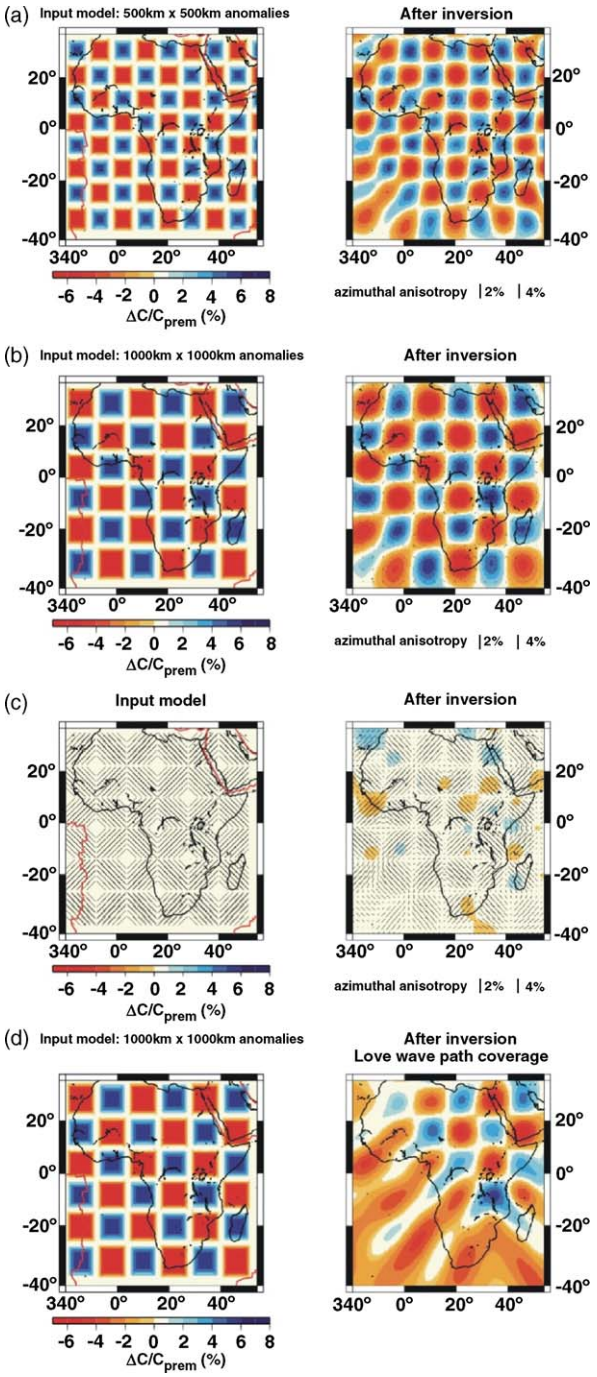

Fig. 7. Four synthetic tests (synthetic model on the left, models after inversion on the right) for Rayleigh wave path coverage (a)–(c) and Love wave path coverage (d). (a), (b) and (d): The synthetic model has fast and slow anomalies of $5^\circ \times 5^\circ$ (a) and $10^\circ \times 10^\circ$ (b and d), respectively, and no anisotropy. (c): The synthetic model has no isotropic-velocity anomalies, but an anisotropy pattern in cells of $10^\circ \times 10^\circ$ with the fast axis oriented N45E and N-45E.

four of the resolution tests. Fig. 7a–c correspond to the Rayleigh wave path coverage. In Fig. 7a and b, the synthetic model displays fast and slow anomalies of 500 km × 500 km and 1000 km × 1000 km, respectively, and no anisotropy. After inversion, the input model is well recovered beneath Africa without trade-off between isotropic-velocity and anisotropy parameters. In Fig. 7c, the synthetic model displays no isotropic-velocity anomalies, but there is an anisotropy pattern in cells of 1000 km × 1000 km with fast axis oriented N45E and N-45E. The model is well recovered beneath Africa and the trade-off between velocities and anisotropy parameters is less than 0.5%. Fig. 7d corresponds to the Love wave path coverage and shows that phase velocity anomalies 1000 km wide are correctly recovered beneath Africa, except at the West and the South. These tests show that our path coverage permits resolution of structure around 500 km wide for the isotropic-velocity and around 1000 km wide for the anisotropy. Azimuthal anisotropy resolution is uniform below Africa and radial anisotropy (derived from the discrepancy between Rayleigh and Love waves) cannot be recovered at the West and the South of Africa.

Synthetic tests of the Rayleigh and Love wave phase velocity simultaneous inversion versus depth can be found in Silveira and Stutzmann (2002) and show that the vertical smearing of the anomalies does not exceed 30 km.

References

Ayadi, A., Dorbath, C., Lesquer, A., Bezzegoud, M., 2000. Crustal and upper mantle velocity structure of the Hoggar swell (Central Sahara Algeria). Phys. Earth Planet. Int. 118, 111–123.

Beucler, E., Stutzmann, E., Montagner, J.-P., 2003. Surface-wave higher mode phase velocity measurments, using a roller-coaster type algorithm. Geophys. J. Int. 155 (1), 289–307.

Brown, C., Girdler, R., 1980. Interpretation of African gravity and its implication for the breakup of the continents. J. Geophys. Res. 85, 6443–6455.

Burke, K., 1996. The African plate. S. Afr. J. Geol 99, 341–410.

Camp, V., Roobol, M., 1992. Upwelling asthenosphere beneath western Arabia and its regional implications. J. Geophys. Res. 97, 15255–15271.

Christensen, N., Lundquist, S., 1982. Pyroxene orientation within the upper mantle. Bull. Geol. Soc. Am. 93, 279–288.

Courtillot, V., Jaupart, C., Manighetti, I., Tapponnier, P., Besse, J., 1999. On causal links betwwen flood basalts and continental breakup. Earth Planet. Sci. Lett. 166, 177–195.

Courtillot, V., Davaille, A., Besse, J., Stock, J., 2003. Three distinct types of hotspots in the Earth's mantle. Earth Planet. Sci. Lett. 205, 295–308.

Davaille, A., Stutzmann, E., Silveira, G., Besse, J., Courtillot, V., 2005. Convective pattern in the Indo-Atlantic box. Earth Planet. Inter. Lett. 239, 233–252.

Debayle, E., Leveque, J., Cara, M., 2001. Seismic evidence for a deeply rooted low velocity anomaly in the upper mantle beneath the northeastern Afro/Arabian continent. Earth Planet. Sci. Lett. 193, 423–436.

Debayle, E., Kennett, B., Priesley, K., 2005. Global azimuthal seismic anisotropy and the unique plate-motion deformation of Australia. Nature 433, 509–512.

Dziewonski, A., 1984. Mapping the lower mantle determination of lateral heterogeneity in P velocity up to degree and order 6. J. Geophys. Res. 89, 5929–5952.

Dziewonski, A., Anderson, D., 1981. Preliminary reference Earth model (PREM). Phys. Earth Planet. Int. 25, 297–356.

Ebinger, C., Sleep, N.H., 1998. Cenozoic magmatism throughout east Africa resulting from impact of a single plume. Nature 395, 788–791.

Gurnis, M., Mitrovica, J., Ritsema, J., van Heijst, J., 2000. Constraining mantle density structure using geological evidence of surface uplift rates: the case of the African superplume. Geoch. Geophys. Geosyst., 1, doi:10.1029/1999GC000035.

Grand, S., van der Hilst, R., Widiyantoro, S., 1997. Global seismic tomography: a snapshot of convection in the Earth. Geol. Soc. Am. Today 7 (4), 1–7.

Hadiouche, O., Jobert, N., Montagner, J., 1989. Anisotropy of the African continent inferred from surface waves. Phys. Earth Planet. Int. 58, 61–81.

Hager, B., Clayton, R., Richards, M., Comer, R., Dziewonski, A., 1985. Lower mantle heterogeneity, dynamic topography and the geoid. Nature 313, 541–545.

Hartley, R., Watts, A., Fairhead, J., 1996. Isostasy of Africa. Earth Planet. Sci. Lett. 137, 1–18.

Hofmann, C., Courtillot, V., Feraud, G., Rochette, P., Yirgu, G., Ketefo, E., Pik, R., 1997. Timing of the Ethiopian flood basalt event and implications for plume birth and global change. Nature 389, 838–841.

Lithgow-Bertelloni, C., Silver, P., 1998. Dynamic topography, plate driving forces and the African superswell. Nature 395, 269–272.

Marty, B., et al., 1993. He, Ar, Sr, Nd and Pb isotopes in volcanic rocks from Afar: evidences for a primitive mantle component and constraints on magmatic sources. Geochem. J. 27, 219–228.

Marty, B., Pik, R., Gezahegn, Y., 1996. Helium isotopic variations in Ethiopian plume lavas: nature of magmatic sources and limit on lower mantle contribution. Earth Planet. Sci. Lett. 144, 223–237.

Mc Nutt, M., 1998. Superswells. Rev. Geophys. 36, 211–244.

Mégnin, C., Romanowicz, B., 2000. A model of shear velocity in the mantle from the inversion of waveforms of body, surface and higher mode waveforms. Geophys. J. Int. 143, 709–728.

Montagner, J.-P., 2002. Upper mantle low anisotropy channels below the pacific plate. Earth Planet. Sci. Lett. 202, 263–274.

Montagner, J.-P, 1986. Regional three-dimensional structures using long-period surface waves. Annales Geophysicae 4, 283–294.

Montagner, J., Nataf, H., 1986. A simple method for inverting the azimuthal anisotropy of surface waves. J. Geophys. Res. 91, 511–520.

Montagner, J.-P., Jobert, N., 1988. Vectorial tomography. II. Application to the Indian Ocean. Geophys. J. R. Astron. Soc. 94, 309–344.

Montagner, J.-P, Marty, B., Stutzmann, E., Sicilia, D., Cara, M., Pik, R., Sebai, A., Lévêque, J.-J., Roult, G., Beucler, E., Debayle, E., submitted for publication. Two types of mantle plumes beneath Africa revealed by seismic tomography and helium isotope geochemistry, Geophys. Res. Lett.

Mooney, W., Laske, G., Masters, T., 1998. CRUST 5.1: A global crustal model at $5^\circ \times 5^\circ$. J. Geophys. Res. 103, 727–747.

Nataf, H., Ricard, Y., 1996. 3SMAC an a priori tomographic model of the upper mantle based on geophysical modelling. Phys. Earth Planet. Int. 95, 101–122.

Ni, S., Helmberger, D., 2003. Seismological constraints on the South African superplume could be the oldest distinct structure on Earth. Earth Planet. Sci. Lett. 206, 119–131.

Nicolas, A., Christensen, N., 1987. Formation of anisotropy in upper mantle peridotites—a review, composition, structure and dynamics of the lithosphere-asthenosphere system, Fuchs and Froidevaux. AGU, 111–123.

Nyblade, A., Robinson, S., 1994. The African superswell. Geophys. Res. Lett. 21, 765–768.

Reagan, J., Anderson, D., 1984. Anisotropic models of the upper mantle. Phys. Earth Planet. Int. 35, 22–263.

Richards, M., Duncan, R., Courtillot, V., 1989. Flood basalts and hotspot tracks: plume heads and tails. Science 246, 103–107.

Ritsema, J., van Heijst, H.J., 2000a. Seismic imaging of structural heterogeneity in Earth's mantle: evidence for large-scale mantle flow. Sci. Progress 83, 243–259.

Ritsema, J., Van Heijst, H., 2000b. New seismic model of the upper mantle beneath Africa. Geology 28, 63–66.

Ritsema, J., Nyblade, A., Owens, T., Langston, C., Van Decar, J., 1998. Upper mantle seismic velocity structure beneath Tanzania, East Africa implication for the stability of cratonic lithosphere. J. Geophys. Res. 103, 21201–21213.

Ritsema, J., Van Heijst, H., Woodhouse, J., 1999. Complex shear wave velocity structure imaged beneath Africa and iceland. Science 286, 1925–1928.

Romanowicz, B., Gung, Y., 2002. Superplumes from the core-mantle boundary to the lithosphere; implications for the heat flux. Science 296, 513–516.

Rogers, N.R., Macdonald, J., Fitton, R., Georges, M., Smith, Barreiro, B., 2000. Two mantle plumes beneath the East African rift system: Sr, Nd and Pb isotope evidence from the Kenya Rift basalts. Earth Planet. Sci. Lett. 176, 387–400.

Silveira, G., Stutzmann, E., 2002. Anisotropic tomography of the Atlantic Ocean. Phys. Earth Planet. Int. 132, 237–248.

Silveira G., Stutzmann, E., Davaille, A., Montagner, J.-P., Mendes-Victor, L., Sebai, A. in press. Azores hotspot signature in the upper mantle. J. Volcano. Geotherm. Res.

Smith, M., Dahlen, F., 1973. The azimuthal dependence of Love and Rayleigh wave propagation in a slightly anisotropic medium. J. Geophys. Res. 78, 3321–3333.

Storey, B., 1995. The role of mantle plumes in continental break up: case histories from Gwondwanaland. Nature 377, 301–308.

Stutzmann, E., Montagner, J.P., 1993. An Inverse technique for retrieving higher mode phase velocity and mantle structure. Geophys. J. Int. 113, 669–683.

Stutzmann, E., Montagner, J.P., 1994. Tomography of the transition Zone from the inversion of higher mode surface waves. Phys. Earth Planet. Int. 86, 99–115.

Tarantola, A., Nercessian, A., 1984. Three-dimensional inversion without blocks. Geophys. J. R. Astron. Soc. 76, 299–306.

Tarantola, A., Valette, B., 1982. Generalized nonlinear inverse problems solved using the least squares criterion. Rev. Geophys. Space Phys. 20, 219–232.

Weeraratne, D., Forsyth, D., Fisher, K., 2003. Evidence of an upper mantle plume beneath the Tanzanian craton from Rayleigh wave tomography. J. Geophys. Res. 108 (B9), 2427, doi10.1029/2002JB002273.

White, R.S., McKenzie, D., 1989. Magmatism at rift zones: the generation of volcanic continental margins and flood basalts. J. Geophys. Res. 94, 7685–7729.

Wilson, M., Guiraud, R., 1992. Magmatism and rifting in western and Central Africa, from late jurassic to recent times. Tectonophysics 213, 203–225.

Woodhouse, J., Girnius, R., 1982. Surface waves and free oscillations in a regionalized earth model. Geophys. J. R. Astron. Soc. 68, 653–673.

Zhao, M., Langston, C., Nyblade, A., Owens, T., 1999. Upper mantle velocity structure beneath southern Africa from modeling regional seismic data. J. Geophys. Res. 104 (B3), 24783–24794.